

Published in final edited form as:

Mol Cell. 2008 June 20; 30(6): 667–677. doi:10.1016/j.molcel.2008.05.008.

The mechanism of a neurotransmitter:sodium symporter – inward release of Na⁺ and substrate is triggered by substrate in a second binding site

Lei Shi^{1,*}, Matthias Quick^{2,4,*}, Yongfang Zhao², Harel Weinstein¹, and Jonathan A. Javitch^{2,3,4,†}

¹Department of Physiology and Biophysics and the HRH Prince Alwaleed Bin Talal Bin Abdulaziz Alsaud Institute for Computational Biomedicine, Weill Medical College of Cornell University, 1300 York Ave, New York, NY 10021, USA

²Center for Molecular Recognition, Columbia University College of Physicians and Surgeons, 630 West 168th Street, New York, NY 10032, USA

³Departments of Psychiatry and Pharmacology, Columbia University College of Physicians and Surgeons, 630 West 168th Street, New York, NY 10032, USA

⁴Division of Molecular Therapeutics, New York State Psychiatric Institute, New York, NY 10032 USA.

Summary

Eukaryotic neurotransmitter:Na⁺ symporters (NSS), targets for antidepressants and psychostimulants, terminate neurotransmission by sodium-driven reuptake. The crystal structure of LeuT_{AA}, a prokaryotic NSS homolog, revealed an occluded state in which one leucine and two Na⁺ ions are bound, but provided limited clues to the molecular mechanism of transport. Using steered molecular dynamics simulations we explored first the extracellular substrate translocation pathway of LeuT and identified a secondary substrate binding site in the extracellular vestibule comprised of residues shown recently to participate in binding tricyclic antidepressants. The same protocol served to outline the intracellular transport pathway. Radiotracer binding and flux experiments showed that the binding sites can be occupied simultaneously by substrates. Binding of substrate to the secondary site allosterically triggers intracellular release of Na⁺ and substrate from the primary site, thereby functioning as a “symport-effector”. Because tricyclic antidepressants bind differently to this secondary site, they do not promote substrate release from the primary site, and thus act as symport uncouplers and inhibit transport.

Introduction

Neurotransmitter:sodium symporters (NSSs) play an essential role in the nervous system by terminating synaptic transmission and recycling neurotransmitters for reuse (Rudnick, 2002). These proteins are secondary active transporters that utilize the Na⁺ gradient across the plasma

© 2008 Elsevier Inc. All rights reserved.

†Correspondence: jaj2@columbia.edu; Ph.: 212-305-7308; Fax: 775-898-5133.

*These authors contributed equally.

Publisher's Disclaimer: This is a PDF file of an unedited manuscript that has been accepted for publication. As a service to our customers we are providing this early version of the manuscript. The manuscript will undergo copyediting, typesetting, and review of the resulting proof before it is published in its final citable form. Please note that during the production process errors may be discovered which could affect the content, and all legal disclaimers that apply to the journal pertain.

membrane to catalyze the uptake of a variety of neurotransmitters from the extracellular milieu against their concentration gradient in a cotransport (symport) mechanism (Torres *et al.*, 2003). NSS substrates include biogenic amines, such as dopamine, norepinephrine, and serotonin, as well as amino acids (γ -aminobutyric acid, glycine, and proline) and osmolytes (betaine and creatine) (Sonders *et al.*, 2005). The transporters for the biogenic amines dopamine, norepinephrine, and serotonin (DAT, NET, and SERT, respectively) are of particular interest because they are targeted by numerous drugs, including the widely abused psychostimulants cocaine and amphetamine (Amara and Sonders, 1998), as well as antidepressants (Iversen, 2006).

Genes encoding more than 200 putative NSS-homologs have been computationally identified in prokaryotic genomes (Beuming *et al.*, 2006), and several of these, including TnaT (Androutsellis-Theotokis *et al.*, 2003), LeuT (Yamashita *et al.*, 2005), Tyl1 (Quick *et al.*, 2006), and MhsT (Quick and Javitch, 2007) were shown to be Na⁺-dependent amino acid transporters. The crystal structure of LeuT at 1.65 Å resolution revealed an occluded binding pocket with L-leucine (Leu) and two Na⁺ ions, Na1 and Na2, complexed within an extensive network of backbone and side chain interactions, which for Na1 also includes the carboxylate of the bound substrate Leu (Yamashita *et al.*, 2005).

A stoichiometry of 2 Na⁺:1 substrate molecule per transport cycle has been inferred for most NSS (Gu *et al.*, 1994), and this has been supported by direct flux experiments in GAT-1 (Krause and Schwarz, 2005). It is likely that coordinated conformational changes couple the movement of Na⁺ down its electrochemical gradient to the uphill movement of substrate (Jardetzky, 1966). We have shown (Quick *et al.*, 2006) that Na⁺ produces conformational changes consistent with an “outward-facing” conformation, and that its absence promotes increased accessibility of cytoplasmic residues consistent with an “inward-facing” conformation of the transporter. Nonetheless, how these changes might drive transport remained a mystery.

The dynamic properties of protein-ligand interaction complexes have been shown to be well described with the current methods of molecular dynamics (MD) simulations (Karplus and Kuriyan, 2005; Kong and Karplus, 2007). However, characterization of the complex conformational rearrangements associated with physiologically relevant allosteric mechanisms such as transport by NSS, requires other types of simulation approaches, capable of describing dynamics involving barrier crossings. Therefore, we have used steered MD (SMD) simulations (Isralewitz *et al.*, 2001) to study the dynamics of ligand movement in LeuT. SMD had been used to simulate unbinding or unfolding events in several biomolecular systems, e. g., LacY (Jensen *et al.*, 2007). We used this approach to simulate ligand motion in LeuT by pulling the substrate along a simulated pathway. The energy barrier crossings are accelerated by this SMD procedure through the application of external forces. Thus, nanoseconds trajectories of SMD will reasonably simulate molecular behavior during the natural transport process (Jensen *et al.*, 2007), such as transport by NSS, in which turnover occurs over hundreds of milliseconds to seconds.

Combining the computational studies with experimental analysis of dissociation kinetics, transport, and binding, we were able to probe the molecular mechanism of LeuT-mediated substrate translocation. Our findings identified a secondary substrate binding site at the extracellular vestibule of LeuT and revealed the nature of its involvement in the transport mechanism. Very recently, tricyclic antidepressants (TCAs) have been shown to bind to a similar site in LeuT where they were considered to trap the substrate Leu in the occluded binding site (Singh *et al.*, 2007; Zhou *et al.*, 2007). We show here that two substrate molecules can bind simultaneously to the primary and secondary sites, and that binding of substrate in the secondary site is the trigger for inward transport of Na⁺ and substrate from the primary

binding site along the permeation pathway. We propose an allosteric mechanism of Na⁺-coupled symport in which binding of substrate to the secondary site is essential for coupling the energy from the electrochemical ion (Na⁺) gradient to the transport of solutes by the NSS.

Results

Identification of a secondary substrate binding site from steered molecular dynamics simulations

For the SMD simulations we constructed and equilibrated a molecular system consisting of Leu-bound LeuT immersed in a solvated lipid-bilayer, based on the original LeuT crystal structure (Yamashita *et al.*, 2005). At the end of a 24 ns unconstrained equilibration, the LeuT model was very similar to the LeuT crystal structure (RMSD of 1.4 Å), and the transmembrane segments (TMs) 1, 3, 6, and 8 were even closer to that structure (RMSD 0.7 Å). Pulling the substrate from its occluded binding site (termed the primary binding site), known from the LeuT crystal, towards the extracellular milieu with a force applied to the center of mass of the Leu, we identified energy barriers along the simulated path with specific interactions along the pathway. These are mainly ionic interactions and hydrogen bonds between the carboxyl/amine groups of Leu and LeuT residues (for details and representative results from SMD runs see Fig. S1). With the reorganization of the protein environment in the path around the pulled substrate, several of the interactions between the amine group of the substrate and LeuT are severed. This allows the Leu to be repositioned between the aromatic rings of Tyr108^{3.50} and Phe253^{6.53} in a cleft that emerges between TMs 1, 3 and 6, before exiting the primary binding site (for indexing system see Goldberg *et al.*, 2003; Beuming *et al.*, 2006). The most remarkable details of the observed structural response to the relocation in this initial movement are (i) the consistent interaction of the carboxylate of Leu with Tyr108, and (ii) the change in both backbone angles and the rotamer of Phe253, which suggests a gating role for this residue in enabling the Leu side chain to exit the binding site. Results from simulations exploring the role of Na⁺ (see below) further support this role.

Further relocation of the substrate with SMD led to a local equilibrium site where the pulling force drops dramatically, thus identifying a new favorable position. Here, Leu is at ~+10 Å along the Z-axis (relative to the primary Leu binding site defined to be at ~0 Å), and is partially exposed to extracellular bulk water. This site at the extracellular vestibule was termed “the secondary binding site” (Fig. 1A-C), and consists of two components: a hydrophobic pocket composed of Leu29^{1.50}, Tyr107^{3.49}, Ile111^{3.53}, Trp114^{3.56}, Ala319^{EL4}, Phe320^{EL4}, Phe324^{EL4}, and Leu400^{10.44} - which accommodates the Leu side chain - and an ionic cleft composed of the Asp404^{10.48} and Arg30^{1.51} that establish direct ionic interactions with the amine and carboxyl groups of Leu, respectively. Recent direct structural studies show that TCAs bind to a very similar site in the extracellular vestibule of LeuT, with Leu and two Na⁺ remaining bound below the TCA in positions nearly identical to the original crystal structure (Yamashita *et al.*, 2005) in which the secondary site is empty and a water molecule is poised to mediate the interaction between Asp404 and Arg30 (Singh *et al.*, 2007; Zhou *et al.*, 2007).

The impact of Na⁺ on the structure of the binding site

Because substrate binding is Na⁺ dependent (see Fig. S2A), we used MD simulations to explore the structural role of the two Na⁺ bound near the Leu by comparing the *holo* crystal structure to results from simulations of constructs in which both ions were removed (–Na), in the presence (+Leu) or absence (–Leu) of the substrate (Fig. 1D-F). A number of local structural changes are observed to occur in the primary binding site in the absence of both Na⁺ and Leu (–Na/–Leu). These produce a “filling in” of the binding cavity (see Fig. 1 and Supplemental Results). An important role in the physiological mechanism of the transporter is attributable

to these changes, as filling and shielding of the cavity in the absence of Na⁺ is likely to be a feature of an inward-open conformation in which the primary binding site is difficult to access from the extracellular environment. In contrast, we found for the “+Na/-Leu” state that water molecules penetrate the cavity and break the Tyr108 to Ser355^{8,60} hydrogen bond in “-Na/-Leu” by binding to each of them separately. In this manner, the presence of Na⁺ opens access to the primary site for the incoming substrate, consistent with the reported conformational dependence of access to position 3.53 (one helical turn above Tyr108) in the biogenic amine transporters (Chen and Rudnick, 2000; Loland *et al.*, 2004).

Our 30 ns-long MD simulations cannot reveal all the intervening conformational changes associated with binding of Na⁺ and Leu, but the end points make the trends quite clear: 1) in the absence of Na⁺, the binding site is shielded from the extracellular milieu and no water molecules are found within the cavity (Fig. 1D, F); 2) the presence of Na⁺ in the Na1 site organizes/orients TM1 and TM6 (e.g., the Gly26^{1,47}-Phe253 interaction), which facilitates an opening to the extracellular milieu and the entry of water molecules into the site (Fig. 1E, F); 3) the additional presence of the bound substrate (“+Na/+Leu”, as in the LeuT crystal structure) protects the primary binding site from direct access from the extracellular milieu through its network of interactions (e.g., with Phe253).

Experimental evidence for two leucines bound simultaneously to the primary and the secondary site

To probe the role of the secondary site for Leu observed in the computational studies, we asked whether two substrate molecules can bind simultaneously to the primary and secondary sites and, if so, what the mechanistic implications would be for the function of the transporter. Computational simulations starting from the end of an equilibration trajectory of the crystal structure of LeuT (Yamashita *et al.*, 2005) indicated the feasibility of double occupancy, with a second Leu positioned in the secondary binding site identified in the SMD simulation. The 30 ns simulation converged, with the ligand maintaining its position unchanged for >10 ns in a binding pose in which it interacts directly with Leu400 and Ile111 (Fig. S8). Therefore, to create constructs with potentially impaired binding in the secondary binding site, we introduced, one at a time, two mutations: I111C and L400C.

Experimentally, we used a scintillation proximity binding assay (SPA) we described recently (Quick and Javitch, 2007) to quantify the binding of ³H-Leu to purified LeuT in detergent (avoiding the potential complications of removing unbound ³H-Leu). Notably, residual bound Leu would greatly complicate analysis of the stoichiometry of substrate binding. The single Leu bound in the high resolution structure of LeuT (Yamashita *et al.*, 2005) must have come from the bacterial growth media and thus remained bound for several days while LeuT was purified in the absence of Leu (Yamashita *et al.*, 2005). We found, however, that extensive washing of LeuT-containing membranes in the absence of Na⁺ removed bound Leu and created an *apo*-LeuT that has the capacity to bind nearly twice as much ³H-Leu as membranes washed in the presence of Na⁺ (Fig. S2B). Membranes washed in the absence of Na⁺ were used in all subsequent experiments.

At 100 nM ³H-Leu the secondary site mutants I111C and L400C exhibited ~50% of the ³H-Leu binding observed for WT (Fig. 2A). Remarkably, in WT the stoichiometry at saturating Leu concentration was 1.8±0.1 Leu per LeuT with an EC_{50}^{Leu} of 70±7 nM (Fig. 2B, n=3). In contrast, ³H-Leu bound to I111C and L400C with a stoichiometry of 1.0±0.1 and 0.9±0.1, and an EC_{50}^{Leu} of 105±18 nM and 68±11 nM, respectively (Fig. 2B, n=3). Addition of the TCA clomipramine (CMI) at 1 mM decreased the equilibrium binding of ³H-Leu to WT by 48±3 % (n=4; Fig. 2C), but had no effect on equilibrium binding to L400C (Fig. 2D) or I111C (data not shown). Taken together, these results are consistent with our hypothesis that Leu can bind

simultaneously to the primary binding site and a secondary site. That this secondary site is indeed the site identified in the SMD analysis is supported both by the apparent loss of the second Leu binding in the secondary site mutants, and by the ability of the TCA - which binds to the secondary site (Singh *et al.*, 2007; Zhou *et al.*, 2007) - to inhibit binding only to WT, but not to constructs that cannot bind ^3H -Leu in the mutated secondary site.

Dissociation experiments reveal a kinetic trapping of Leu

After 30 min incubation, specifically-bound ^3H -Leu dissociated rapidly from WT or the second site mutants regardless of whether the dilution was in the presence (Figs. 3A & S3A) or absence of Na^+ (Figs. 3B & S3B). Remarkably, we observed that only about 50% of bound ^3H -Leu was released when the incubation was carried out for 3-5 h prior to dilution (data not shown). After prolonged incubation (typically 16 h – see Supplemental Experimental Procedures), dissociation from WT into buffer containing Na^+ led to rapid loss of bound ^3H -Leu that leveled off at $52 \pm 3.7\%$ ($n=4$) of total binding (Fig. 3C). Thus, it appears that after prolonged incubation, one Leu remains trapped, whereas a second Leu is readily released. This kinetically-trapped state likely corresponds to the one visualized in the LeuT crystal structure (Yamashita *et al.*, 2005), and thereby provided us an opportunity to explore the components of the physiological mechanism of transport. Interestingly, ^3H -Leu did not dissociate from the mutants in this state, when diluted into buffer containing Na^+ (Figs. 3C & S3C). This is consistent with the binding and trapping of a single Leu because at the tested concentration ^3H -Leu cannot bind to the mutated secondary site. WT differs from the mutants also when release is measured in the absence of Na^+ (mimicking intracellular physiological conditions), because then all bound ^3H -Leu dissociates from WT (Fig. 3D), whereas in the mutants all the bound ^3H -Leu remains trapped (Figs. 3D & S3D).

The observed change in ^3H -Leu dissociation pattern after prolonged incubation led us to hypothesize that S1 (the substrate in the primary binding site) becomes kinetically trapped in an occluded form of the transporter, as evidenced by the presence of S1 in the crystal structure obtained after purification in the absence of Leu. We further inferred that in order to achieve release of S1, a second substrate (S2) must bind to the secondary site, but that release of S1 cannot occur if Na^+ is present (see below experiments supporting the details concerning Na^+ binding and dissociation). In contrast, S2 is readily bound and released from the secondary site, even in the kinetically trapped state. These rules are consistent with *i*) the observed dissociation of both S1 and S2 from WT when the transporter is diluted in the absence of Na^+ , as well as with *ii*) the persistent trapping of S1 but not S2 when the transporter is diluted in the presence of Na^+ . Based on the behavior of the secondary site mutants, we predicted that emptying the S2 binding site by diluting LeuT-WT in the presence of Na^+ (as in Fig. 3C) would prevent the release of S1 upon subsequent dilution into no Na^+ ; this was indeed found to be the case (Fig. 3E). The mutants, which cannot bind S2, mimicked this phenotype, as S1 remained trapped both in the presence and in the absence of Na^+ (Figs. 3E & S4A).

In further support of these mechanistic rules, in the absence of Na^+ , when 250 nM unlabeled Leu was added to the WT LeuT trapped state with S1 bound, the secondary site was filled (S2 bound), causing complete release of trapped ^3H -Leu (S1) (Fig. 3E). In contrast, the identical addition of Leu was without effect in the mutants that disrupt the secondary site (Fig. 3E). Interestingly, dissociation from such a mutant, LeuT-L400C, into a very high concentration (1 mM) of Leu recapitulated WT behavior and released ^3H -Leu from the S1 binding site (Fig. S4A). This suggests that the mechanism of release remains activatable in the mutants if the concentration of Leu is high enough to fill the mutated secondary site.

In the presence of Na^+ , when 250 nM unlabeled Leu was added to the WT trapped state with S1 bound, S1 remained trapped (Fig. 3G) despite the rebinding of S2 (Fig. 3H). This is consistent with the rule (substantiated by the physiological conditions of low intracellular

Na⁺) that S1 cannot be released in the presence of Na⁺ (see below). Supporting this hypothesis, dilution of this species in Na⁺-free medium led to release of both S1 (Fig. 3G) and of S2 (Fig. 3H). Notably, binding of CMI to the secondary site does not have the same effect as substrate. Incubation with 1 mM CMI, which occupies the secondary site (Singh *et al.*, 2007; Zhou *et al.*, 2007) and competes for binding with S2 (but not S1) (Fig. 2C, D), completely blocked dissociation of S1 in the absence of Na⁺ (Fig. 3F). Thus, occupation of the secondary site by a TCA is functionally similar to an empty or mutated secondary site, consistent with the behavior of these compounds as transport inhibitors.

Measuring binding of ²²Na⁺ to LeuT reveals trapping by Leu

Given the physiological function of the NSS, we expected that different patterns of release and exchange of the two sodiums account for the differential dissociation of ³H-Leu in Na⁺/Na⁺-free media. Therefore, we used the SPA to measure ²²Na⁺ binding directly (Fig. S5).

Competition with unlabeled Na⁺ revealed an $IC_{50}^{Na^+}$ of 10.2±1.2 mM with a Hill coefficient of 1.9±0.1 in WT (Fig. 4A) and an $IC_{50}^{Na^+}$ of 10.0±0.1 mM and a Hill coefficient of 2.0±0.1 in L400C (Fig. 4B), consistent with an $EC_{50}^{Na^+}$ of 10.3 ± 1.3 and a Hill coefficient of 1.9 ± 0.3 for WT and an $EC_{50}^{Na^+}$ of 10.1 ± 3.0 with a Hill coefficient of 1.7 ± 0.1 for L400C for Na⁺ stimulation of ³H-Leu binding (Fig. S2A).

After prolonged incubation in the absence of Leu, ²²Na⁺ rapidly and completely dissociated from both WT (Fig. 4C) and L400C (Fig. 4D) upon dilution, regardless of the presence or absence of unlabeled Na⁺. When prolonged incubation with ²²Na⁺ was performed in the presence of Leu, ²²Na⁺ also dissociated completely upon dilution of WT in the absence of Na⁺ (which releases both S1 and S2, Fig. 3D) (Fig. S6A). However, when the secondary site mutant L400C, in which S1 remained trapped (Fig. 3D), was diluted in the absence of Na⁺, 47 ± 6 % (n=4) of ²²Na⁺ was also trapped, consistent with the release of one Na⁺ ion and the trapping of one Na⁺ ion together with S1 (Fig. S6B).

We hypothesized that after trapping S1 in WT LeuT, removal of S2 would have an effect similar to that of the secondary site mutants, in that one Na⁺ ion would also become trapped. To test this prediction, WT was bound overnight in the presence of Leu and ²²Na⁺, which led to the trapping of S1. The transporter was diluted into buffer containing ²²Na⁺, which led to release of S2 (Fig. 3C). When this complex subsequently was diluted in the absence of Na⁺, 47±5 % (n=3) of ²²Na⁺ remained bound (Fig. 4E), again consistent with the dissociation of one Na⁺ and the trapping of one Na⁺ along with S1. Similar results were observed in L400C (Fig. 4F). However, only in WT, but not in the mutant, was the trapped Na⁺ released by subsequent addition of 250 nM Leu and binding of S2; this occurred only in the absence of additional Na⁺ (Fig. 4E), but not in the presence of Na⁺ (Fig. 4F).

These findings reveal a mechanism in which one Na⁺ and S1 are trapped in the primary site in the absence of bound S2, but one Na⁺ is readily released, presumably to the intracellular side. We have not determined directly which Na⁺ (Na1 or Na2) is trapped and which is released, but because only Na1 directly contacts the carboxylate of trapped S1 whereas Na2 is closer to intracellular bulk water, we reasoned that Na1 is the trapped ion and Na2 is released. To evaluate this prediction from a thermodynamic perspective, we compared the free energy for Na1 and Na2 calculated in different conformational states using free energy perturbation (FEP) calculations (see Supplemental Experimental Procedures). The calculations also included the solvation energy of Na⁺ in a water box (−92.0 ± 0.1 kcal/mol, which agrees with previously reported experimental and computed values; Grossfield *et al.*, 2003). In the absence of substrate (−S1/−S2/+Na1/+Na2), Na1 and Na2 have free energy of −104.2, and −101.2 kcal/mol, respectively, but with S1 in the primary binding site (+S1/−S2/+Na1/+Na2), the binding of

Na2 is weakened (by >4 kcal/mol), whereas Na1 is significantly stabilized (by >8 kcal/mol). Notably, the binding of the substrate(s) lowers the free energy of bound Na2 to resemble that of Na⁺ in water, which makes Na2 a much more likely candidate for release. In the absence of Na2 (+S1/−S2/+Na1/−Na2), Na1 is even more stable (by 13 kcal/mol), but the conformational change produced by S2 binding (+S1/+S2/+Na1/−Na2) destabilizes Na1 (by 5 kcal/mol), consistent with the role of S2 in releasing trapped S1 and Na1 in the absence of Na2.

Substrate binding to the secondary site has a role in Na⁺-coupled transport

Alanine (Ala) is transported more efficiently by LeuT than is Leu (Ryan and Mindell, 2007; Singh *et al.*, 2007; Fig. 5A, B). As a further step in elucidating the physiological relevance of the mechanism we revealed, we extended the study to the effects of Ala on the functions of LeuT. As determined by SPA, the binding stoichiometry of ³H-Ala to purified LeuT-WT at saturation was 2.0±0.3 (n=3) Ala per LeuT, whereas for purified L400C it was 1.0±0.2 (n=3), consistent with our findings with Leu. For WT, the ³H-Ala binding curve was complex with an EC_{50}^{Ala} of 28.4±5.4 μM (n=3), whereas the curve for L400C was consistent with a one-site fit with an EC_{50}^{Ala} of 35.8±12.4 μM (n=3). Unlike Leu, overnight incubation with ³H-Ala did not lead to substrate trapping (data not shown). However, in the absence of Na⁺, 5 μM Ala led to rapid release from WT of trapped ³H-Leu (Fig. 5E) and trapped ²²Na⁺ (Fig. 5F), consistent with the ability of the Ala substrate to bind to the secondary site and trigger release of S1 and Na1. In contrast, 5 μM Ala was unable to promote release of either S1 (Fig. 5E) or Na1 (Fig. 5F) from the secondary site mutant L400C.

Functional reconstitution of purified WT and mutant LeuT into proteoliposomes (PLs) was confirmed by ³H-Ala binding (Fig. 5C), which was fully consistent with the binding results in detergent (data not shown). However, despite successful reconstitution, essentially no ³H-Ala transport into PLs was observed in the secondary site mutants (Fig. 5D), in marked contrast to WT. This lack of transport by the secondary site mutants indicates that substrate binding to the secondary site is essential for physiological Na⁺-coupled transport, and not only for the release of Na1 and S1 in binding assays.

Inward release of S1 in response to S2 binding

To establish that release of trapped S1 was indeed, as depicted in Fig. 6, from the cytoplasmic face of the transporter, and thus a measure of the physiological inward release step during the transport cycle, we carried out additional experiments in PLs in which LeuT-WT was reconstituted in an outside-out configuration (see Supplemental Experimental Procedures). ³H-Leu was bound to the PLs under conditions that allowed trapping of S1. The PLs were diluted in the presence of Na⁺, which led to release of S2, but preserved binding of S1 (Fig. 5G), just as we observed in detergent (Fig. 3C). Subsequent dilution in Na⁺-free medium was without further effect on ³H-Leu binding (trapped S1) (Fig. 5G), as was also the case in detergent (Fig. 3E). In contrast to our results in detergent, however, in the PLs, subsequent addition of 250 nM Leu in the absence of Na⁺ did not lead to loss of radioactivity (Fig. 5G), since S1 was released to the interior of the PLs and retained upon filtration. That the ³H-Leu (S1) had indeed been released to the inside of the PLs was confirmed by their detergent-permeabilization, which led to rapid loss of ³H-Leu upon binding of S2 (Fig. 5G). The behavior of the secondary site mutant I111C in the PLs was identical to that in detergent, as S1 remained trapped and was not released (Fig. 5H).

To define the intracellular transport pathway through which S1 is released to the cytoplasm, we used an intracellular SMD pulling protocol, as described in the Experimental Procedures. Importantly, in the absence of Na2, it is easier to pull the substrate towards the cytoplasm, as becomes evident from a comparison of force profiles (data not shown). This is consistent with

the structural information showing that Na2 is located at the junction of TM1, TM6, and TM8 and likely contributes to the stabilization of the relative orientation of these helices (Fig. 6).

In the inward-pulling trajectory, the substrate is surrounded by elements of the N-terminus (NT), TM4-IL4-TM5, and TM8 (specifically by Trp8^{NT}, Leu183^{4.62}, Ile187^{IL2}, Ile191^{5.39}, Ile357^{8.62}, and Ala358^{8.63}). Notably, in SERT the residues corresponding to Ile187^{IL2} and Ile191^{5.39} have been found to be accessible (Zhang and Rudnick, 2005), and the accessibility of the aligned residue at position 8.63 in GAT1, Cys399^{8.63}, is conformationally sensitive (Golovanovsky and Kanner, 1999). The polar portion of Leu interacts directly or through water intermediates with Ala17^{1.38}, Gly20^{1.41}, and Thr354^{8.59} that is conserved as Thr/Ser in prokaryotic NSS and as Asp in eukaryotic NSS. The identity of the residues swept by the pulled substrate in the SMD procedure are consistent with previous mutagenesis and/or accessibility studies in other transporters (Supplemental Table 1), supporting the generality of our findings to other NSS.

The most prominent features of the pathway are described in Figure 6. They are consequences of two main rearrangement groups: one involves the interactions between Arg5^{NT} and Ser267^{IL3}/Tyr268^{IL3}/Asp369^{8.74} (Kniazeff *et al.*, 2008), and the other is a consequence of the dissociation of the interaction of Arg11^{1.32}-Asp274^{IL3}. These relate to the movements of entire segments: TM2-IL1 vs. IL5-TM11 initiated from the pincer-like Pro-kink of TM2 (Sen *et al.*, 2005); TM6-IL3-TM7 and TM1 vs. TM4-IL2-TM5. We observed that the major movements in the protein do not remain localized to the cytoplasmic end of the molecule, but are propagated to the region surrounding the secondary site, and are much more pronounced in the presence of bound S2 than in its absence. These significant dynamic rearrangements allow penetration of water towards the moving substrate (Fig. 6).

Discussion

Our integrated approach of computational MD and SMD simulations combined with corresponding measurements of binding and transport has revealed a functionally essential second substrate binding site in the extracellular vestibule of LeuT. This vestibule comprises a hydrophobic portion that interacts with the substrate side chain, and a hydrophilic portion that is partially exposed to bulk water. Residues aligned with the secondary site residues Leu400^{10.44} and Ile111^{3.53} have been suggested to be involved in the substrate translocation pathway in other NSS homologs based on cysteine accessibility data (Keller *et al.*, 2004; Chen and Rudnick, 2000; Loland *et al.*, 2004).

We have now established experimentally that substrate can bind simultaneously to the primary and secondary binding sites. Substrate binding to this secondary site, which we have termed the “symport-effector site”, couples the gradient-determined movement of Na⁺ to the movement of substrate against its concentration gradient. In this novel mechanism of Na⁺-coupled symport, the second substrate molecule, in the secondary binding site, triggers release of Na⁺ and substrate from the primary binding site when Na⁺ concentrations are low at the other (cytoplasmic) side. Thus, the combined computational and experimental findings led to a proposed allosteric mechanism for Na⁺-coupled symport by this class of proteins, as outlined in Fig. 7. According to this mechanism, the transport cycle starts when extracellular Na⁺ enables the binding of Na1 and Na2 and the entry of water into the binding site, which reorganizes the primary binding site and shifts the conformational equilibrium of the transporter to an outward-facing conformation. Thus, Na⁺ binding increases the affinity of substrate for the primary binding site, and no binding was observed in the absence of Na⁺ for Leu (Fig. S2A) or Ala (data not shown). When substrate is in the primary binding site, the extracellular gate - composed of Phe253^{6.53}, Arg30^{1.51} and Asp404^{10.48} - closes and forms a stable interaction, trapping the substrate in the primary site. When Na1 and S1 are occluded in

the primary site, we find that the free energy of binding for Na2 is close to its aqueous solvation energy, and that Na2 is readily released to the intracellular side. Since the intracellular Na⁺ concentration is low, Na2 should rebinding only very rarely from the intracellular milieu. But Na1 and S1, which are in direct contact in the crystal structure, remain in the primary site until a second substrate molecule (S2) binds to the symport-effector site and triggers the release of Na1 and substrate from the primary site by disrupting a stabilizing network of interactions (see Fig. S8). Both are released from the intracellular side with the support of water penetration (see Fig. 6) since the extracellular gate is closed and S2 is bound above it. The physiological Na⁺ gradient enables the reentry of Na⁺ from the extracellular milieu, which in turn facilitates the reorganization of the outward-facing state. It is likely that the local “effective high concentration” of substrate due to binding in the vestibule helps reload the primary binding site as it is reorganized by Na⁺, thereby facilitating the next transport cycle. This mechanism for a secondary transporter supports directional transport of substrate powered by the energy of the Na⁺ gradient.

The key role of S2 in this mechanism is substantiated by our findings that mutations of the symport-effector site that abolish substrate binding there lead to virtually complete loss of transport. Similarly, the transport-inhibiting TCAs, such as CMI, that bind in the secondary site are symport-uncouplers given their ability to compete with, but not mimic, binding of substrate in the symport-effector site. This is likely due to the differences in modes of binding between Leu and CMI in the secondary binding site, which are significant (Fig. S8D-G). Although our findings are consistent with the ability of TCAs to inhibit roughly half of substrate binding (Zhou *et al.*, 2007; Fig. 2C), we cannot define them as non-competitive antagonists because they compete directly with substrate for binding to the secondary site in LeuT, and possibly in NET and SERT as well (Zhou *et al.*, 2007).

The experimental studies underlying the NSS transport mechanism proposed here were made possible by the fact that prolonged binding of Leu and Na⁺ leads to a trapped occluded state likely represented by the crystal structure (Yamashita *et al.*, 2005). This stable kinetically-trapped state is likely to correspond to what is more typically a transient intermediate conformation in other NSS. Indeed, Ala, which is reasonably well transported by LeuT in a Na⁺-coupled manner, is not trapped within the primary binding site of LeuT, but functions as an efficient symport-effector at the secondary site (see Fig. 5E, F). Therefore, the physiological function of other NSS is likely to follow the mechanistic model described here.

The allosteric mechanism by which binding of a second substrate to the symport-effector site facilitates release of Na1 and S1, is likely complex and involves changes in specific interaction networks (see Fig. S8). Experimentally, evidence for coupling between the primary and secondary sites may be apparent in the ³H-Ala binding data and in the fact that the K_m^{Ala} for Ala transport is ~35-fold lower than the EC_{50}^{Ala} for Ala binding. The actual “affinity” of the secondary site for Ala may be higher than observed in an equilibrium binding assay in which binding of Ala to the secondary site may lower its affinity for the primary site. Similar effects in other NSS may complicate measuring substrate affinity in binding assays with radiolabeled inhibitors. Indeed, this mechanism might account for the lower apparent affinity of biogenic amine substrates determined in competition binding experiments when compared with their apparent K_m for transport (Javitch *et al.*, 1984). Moreover, different affinities of substrates for the primary and symport-effector sites in various transporters may explain a number of other puzzling phenomena, such as inhibitors having different potencies against different substrates (Cesura *et al.*, 1987). Indeed the ability of serotonin to noncompetitively inhibit dopamine transport by SERT (Sonders *et al.*, in preparation) suggests that this happens in human NSS, implying that SERT and other biogenic amine transporters function as described here through an allosteric mechanism involving the two conformationally-coupled substrate sites.

Experimental Procedures

Preparation of LeuT, scintillation proximity assay (SPA), transport and binding in proteoliposomes

Expression, purification, and preparation of recombinant LeuT (containing an N-terminal 10-histidine tag) were performed as described in Supplemental Experimental Procedures. All binding experiments involving purified LeuT variants were performed using the SPA technique, which allows rapid and sensitive measurement of radioisotope binding without the need for a separation step, as well as transport and binding studies in proteoliposomes were assayed as described (Quick and Javitch, 2007; see also Supplemental Experimental Procedures for experimental details).

Construction of the simulated system

All the simulations utilized molecular constructs of Leu-bound LeuT (Leu/LeuT) based on the crystal structure (Yamashita *et al.*, 2005). Two residues in EL2 and four residues at the beginning of the N-terminus that were not resolved in the crystal structure were added with Modeller (Sali and Blundell, 1993). All the water molecules were maintained in the full-length LeuT model building. The simulation systems with the transporter molecules immersed in explicit water-lipid bilayer-water explicit solvent models were constructed with VMD (Humphrey *et al.*, 1996) and equilibrated with NAMD (Phillips *et al.*, 2005), following a procedure modified from (Sotomayor and Schulten, 2004). The transporter model was first immersed in a previously equilibrated rectangular patch consisting of 204 POPC molecules (101 on the periplasmic side and 103 on the cytoplasmic side), one 10 Å layer of water on each side, and Na⁺ and Cl⁻ ions corresponding to a concentration of 150 mM NaCl (a total of ~78,000 atoms). The all-atom CHARMM27 force field was used throughout. Constant temperature (310 K) was maintained with Langevin dynamics, and 1 atm constant pressure was achieved using the hybrid Nosé-Hoover Langevin piston method on a flexible periodic cell, with orthogonal pressure components - Px, Py, and Pz (perpendicular to membrane) - computed independently to account for system anisotropy. After 24 ns of free equilibration, the LeuT/Leu system reached a final dimension of ~87×87×98 Å³.

During the equilibration of the protein in its environment the backbones were initially fixed and then harmonically constrained, and water was prevented from penetrating the protein-lipid interface. Constraints were released gradually in four 300-ps steps with force constants of 1, 0.5, 0.1, and 0.01 kcal/(mol·Å²), respectively. The systems with two substrates bound were obtained by restarting from the last snapshot of the 12 ns “+Na/+Leu” trajectory, with the orientation of Leu in the secondary site taken from the equilibration of SMD (see below) results (overlapping waters were removed before 2500 steps of energy minimization).

All the systems were freely equilibrated for at least 24 ns. At least two independent trajectories were collected for each configuration.

Steered Molecular Dynamics (SMD)

The constant velocity SMD algorithm implemented in NAMD (Isralewitz *et al.*, 2001) was used in the study designed to identify the residues lining the translocation pathway by dragging the substrates out of the binding site, either upward or downward, at a chosen slow speed. The protein was constrained along the z-axis (perpendicular to the membrane plane) during the SMD to avoid its movement in response to the force applied to the substrate in this direction. Constraints were applied to TMs 2, 4, 5, 7, and 9-12 – which are not directly involved in substrate binding – in a center of mass scheme. “Center of mass pulling” of the substrate was used because preliminary runs showed that steering force applied to the center of mass, as opposed to Cα or Cβ, caused the least distortion of the substrate (data not shown).

The Leu/LeuT system required on average 48 hours to complete a 2 ns SMD run on a system with 32 Intel Xeon CPU (3.20 GHz). For production runs, the velocity was 0.005 Å/ps, with a force constant of 4 kcal/(mol·Å²) in a pulling direction perpendicular to the membrane plane. During each 2 ns of pulling, constant pressure was maintained with the hybrid Nosé-Hoover Langevin piston method but the system was decoupled from any thermostat. At the end of each such period the system was coupled to a Langevin thermostat and was equilibrated for at least 8 ns at 310 K.

In the SMD runs the substrate needs to be pulled slowly enough to allow the transporter to equilibrate in the presence of the substrate in its new position, and to reach convergence in terms of the orientation of substrate in the transporter. This requirement is even stronger when the substrate is pulled towards the intracellular side, because the starting (crystal) structure represents an “inward-closed” state. Consequently, we applied two strategies: 1) we divided the inward pulling into three stages: in the first pulling stage, SMD was carried out for 2 ns, followed by 4 ns of MD; in the second, 2 ns of SMD 2 was followed by 20 ns of MD equilibration; finally the substrate is pulled out of the transporter (Jensen *et al.*, 2007); 2) we used gradually reduced pulling velocities in each pulling stage, so that the substrate is subjected to a moderate force for longer times (producing small substrate movements).

Free Energy Perturbation

The Free Energy Perturbation (FEP) calculations were carried out with NAMD and the same simulation systems with explicit solvent as described in Experimental Procedures. For each of the FEP computations the coupling parameter λ varied from 0 to 1 by increments of 0.05 (0.0-1.0) for a total 400 ps for the full annihilation of a Na⁺ ion. In the hysteresis tests the results differed from the annihilation in the same interval by < 0.5 kcal/mol. Each reported value is the average of at least two runs starting from different points (after at least 10 ns) of the MD trajectories.

Using the restraining potential approach (Wang *et al.*, 2006), a potential representing the interaction of the Na⁺ atom being annihilated with the binding residues at the Na1 or Na2 site was applied, with the form $\frac{1}{2}[k_t(r_1-r_{10})+k_t(r_2-r_{20})+k_a(\theta-\theta_0)+k_a(\Phi-\Phi_0)]$. The k_t (100 kcal/mol/Å²) and k_a (100 kcal/mol/rad²) are force constants for the distance and angle/dihedral restraints, respectively; r_{10} , r_{20} , θ_0 , and Φ_0 are the reference values averaged from the equilibrated periods of corresponding trajectories (Wang *et al.*, 2006). The resulting restraining energy values were calculated to be in the range of 2.0 to 3.4 Kcal/mol, i.e., 2-3% of the free energies of the Na⁺ ions calculated with FEP. The final solvation energies were calculated as the algebraic sum of the FEP and restraining energy values.

The aqueous solvation energy of Na⁺ in the simulation system was calculated for direct comparison in a 30×30×30 Å³ water box containing two Na⁺ and two Cl⁻ ions (equivalent to 123 mM NaCl) using exactly the same FEP/MD procedure as above but without restraints.

Supplementary Material

Refer to Web version on PubMed Central for supplementary material.

Acknowledgments

LS carried out the computational work, MQ performed the binding/transport experiments, and YZ performed transport experiments. We thank Lynn Chung for preparation of membranes and Lihua Duan for making the LeuT-II11C and L400C mutants. We thank Arthur Karlin, Amy Newman, and Ming Zhou for helpful discussion and comments on the manuscript. This work was supported by NIH grants DA022413, DA017293, and DA012408.

References

- Amara SG, Sonders MS. Neurotransmitter transporters as molecular targets for addictive drugs. *Drug Alcohol Depend* 1998;51:87–96. [PubMed: 9716932]
- Androutsellis-Theotokis A, Goldberg NR, Ueda K, Beppu T, Beckman ML, Das S, Javitch JA, Rudnick G. Characterization of a functional bacterial homologue of sodium-dependent neurotransmitter transporters. *J Biol Chem* 2003;278:12703–12709. [PubMed: 12569103]
- Beuming T, Shi L, Javitch JA, Weinstein H. A comprehensive structure-based alignment of prokaryotic and eukaryotic neurotransmitter/Na⁺ symporters (NSS) aids in the use of the LeuT structure to probe NSS structure and function. *Mol Pharmacol* 2006;70:1630–1642. [PubMed: 16880288]
- Cesura AM, Ritter A, Picotti GB, Da Prada M. Uptake, release, and subcellular localization of 1-methyl-4-phenylpyridinium in blood platelets. *J Neurochem* 1987;49:138–145. [PubMed: 3495635]
- Chen JG, Rudnick G. Permeation and gating residues in serotonin transporter. *Proc Natl Acad Sci U S A* 2000;97:1044–1049. [PubMed: 10655481]
- Goldberg NR, Beuming T, Soyer OS, Goldstein RA, Weinstein H, Javitch JA. Probing conformational changes in neurotransmitter transporters: a structural context. *Eur J Pharmacol* 2003;479:3–12. [PubMed: 14612133]
- Golovanevsky V, Kanner BI. The reactivity of the gamma-aminobutyric acid transporter GAT-1 toward sulfhydryl reagents is conformationally sensitive. Identification of a major target residue. *J Biol Chem* 1999;274:23020–23026. [PubMed: 10438469]
- Grossfield A, Ren P, Ponder JW. Ion solvation thermodynamics from simulation with a polarizable force field. *J Am Chem Soc* 2003;125:15671–15682. [PubMed: 14664617]
- Gu H, Wall SC, Rudnick G. Stable expression of biogenic amine transporters reveals differences in inhibitor sensitivity, kinetics, and ion dependence. *J Biol Chem* 1994;269:7124–7130. [PubMed: 8125921]
- Humphrey W, Dalke A, Schulten K. VMD: visual molecular dynamics. *J Mol Graphics* 1996;14:33–38. 27–38.
- Isralewitz B, Gao M, Schulten K. Steered molecular dynamics and mechanical functions of proteins. *Curr Opin Struct Biol* 2001;11:224–230. [PubMed: 11297932]
- Iversen L. Neurotransmitter transporters and their impact on the development of psychopharmacology. *Br J Pharmacol* 2006;147(Suppl 1):S82–88. [PubMed: 16402124]
- Jardetzky O. Simple allosteric model for membrane pumps. *Nature* 1966;211:969–970. [PubMed: 5968307]
- Javitch JA, Blaustein RO, Snyder SH. [³H]mazindol binding associated with neuronal dopamine and norepinephrine uptake sites. *Mol Pharmacol* 1984;26:35–44. [PubMed: 6087116]
- Jensen MO, Yin Y, Tajkhorshid E, Schulten K. Sugar transport across lactose permease probed by steered molecular dynamics. *Biophys J* 2007;93:92–102. [PubMed: 17434947]
- Karplus M, Kuriyan J. Molecular dynamics and protein function. *Proc Natl Acad Sci U S A* 2005;102:6679–6685. [PubMed: 15870208]
- Keller PC 2nd, Stephan M, Glomska H, Rudnick G. Cysteine-scanning mutagenesis of the fifth external loop of serotonin transporter. *Biochemistry* 2004;43:8510–8516. [PubMed: 15222762]
- Kniazeff J, Shi L, Loland CJ, Javitch JA, Weinstein H, Gether U. An intracellular interaction network regulates conformational transitions in the dopamine transporter. *J Biol Chem*. 2008 in press.
- Kong Y, Karplus M. The signaling pathway of rhodopsin. *Structure* 2007;15:611–623. [PubMed: 17502106]
- Krause S, Schwarz W. Identification and selective inhibition of the channel mode of the neuronal GABA transporter 1. *Mol Pharmacol* 2005;68:1728–1735. [PubMed: 16150932]
- Loland CJ, Granas C, Javitch JA, Gether U. Identification of intracellular residues in the dopamine transporter critical for regulation of transporter conformation and cocaine binding. *J Biol Chem* 2004;279:3228–3238. [PubMed: 14597628]
- Phillips JC, Braun R, Wang W, Gumbart J, Tajkhorshid E, Villa E, Chipot C, Skeel RD, Kale L, Schulten K. Scalable molecular dynamics with NAMD. *J Comp Chem* 2005;26:1781–1802. [PubMed: 16222654]

- Quick M, Javitch JA. Monitoring the function of membrane transport proteins in detergent-solubilized form. *Proc Natl Acad Sci U S A* 2007;104:3603–3608. [PubMed: 17360689]
- Quick M, Yano H, Goldberg NR, Duan L, Beuming T, Shi L, Weinstein H, Javitch JA. State-dependent conformations of the translocation pathway in the tyrosine transporter Tyt1, a novel neurotransmitter:sodium symporter from *Fusobacterium nucleatum*. *J Biol Chem* 2006;281:26444–26454. [PubMed: 16798738]
- Rudnick, G., editor. Mechanisms of biogenic amine neurotransmitter transporters. 2 edn. Humana Press Inc.; Totowa, New Jersey: 2002.
- Ryan RM, Mindell JA. The uncoupled chloride conductance of a bacterial glutamate transporter homolog. *Nat Struct Mol Biol* 2007;14:365–371. [PubMed: 17435767]
- Sali A, Blundell TL. Comparative protein modelling by satisfaction of spatial restraints. *J Mol Biol* 1993;234:779–815. [PubMed: 8254673]
- Sen N, Shi L, Beuming T, Weinstein H, Javitch JA. A pincer-like configuration of TM2 in the human dopamine transporter is responsible for indirect effects on cocaine binding. *Neuropharmacology* 2005;49:780–790. [PubMed: 16216288]
- Singh SK, Yamashita A, Gouaux E. Antidepressant binding site in a bacterial homologue of neurotransmitter transporters. *Nature* 2007;448:952–956. [PubMed: 17687333]
- Sonders MS, Quick M, Javitch JA. How did the neurotransmitter cross the bilayer? A closer view. *Curr Opin Neurobiol* 2005;15:296–304. [PubMed: 15919190]
- Sotomayor M, Schulten K. Molecular dynamics study of gating in the mechanosensitive channel of small conductance MscS. *Biophys J* 2004;87:3050–3065. [PubMed: 15339798]
- Torres GE, Gainetdinov RR, Caron MG. Plasma membrane monoamine transporters: structure, regulation and function. *Nat Rev Neurosci* 2003;4:13–25. [PubMed: 12511858]
- Wang J, Deng Y, Roux B. Absolute binding free energy calculations using molecular dynamics simulations with restraining potentials. *Biophys J* 2006;91:2798–2814. [PubMed: 16844742]
- Yamashita A, Singh SK, Kawate T, Jin Y, Gouaux E. Crystal structure of a bacterial homologue of Na⁺/Cl[−]-dependent neurotransmitter transporters. *Nature* 2005;437:215–223. [PubMed: 16041361]
- Zhang YW, Rudnick G. Cysteine-scanning mutagenesis of serotonin transporter intracellular loop 2 suggests an alpha-helical conformation. *J Biol Chem* 2005;280:30807–30813. [PubMed: 15994310]
- Zhou Z, Zhen J, Karpowich NK, Goetz RM, Law CJ, Reith ME, Wang DN. LeuT-desipramine structure reveals how antidepressants block neurotransmitter reuptake. *Science* 2007;317:1390–1393. [PubMed: 17690258]

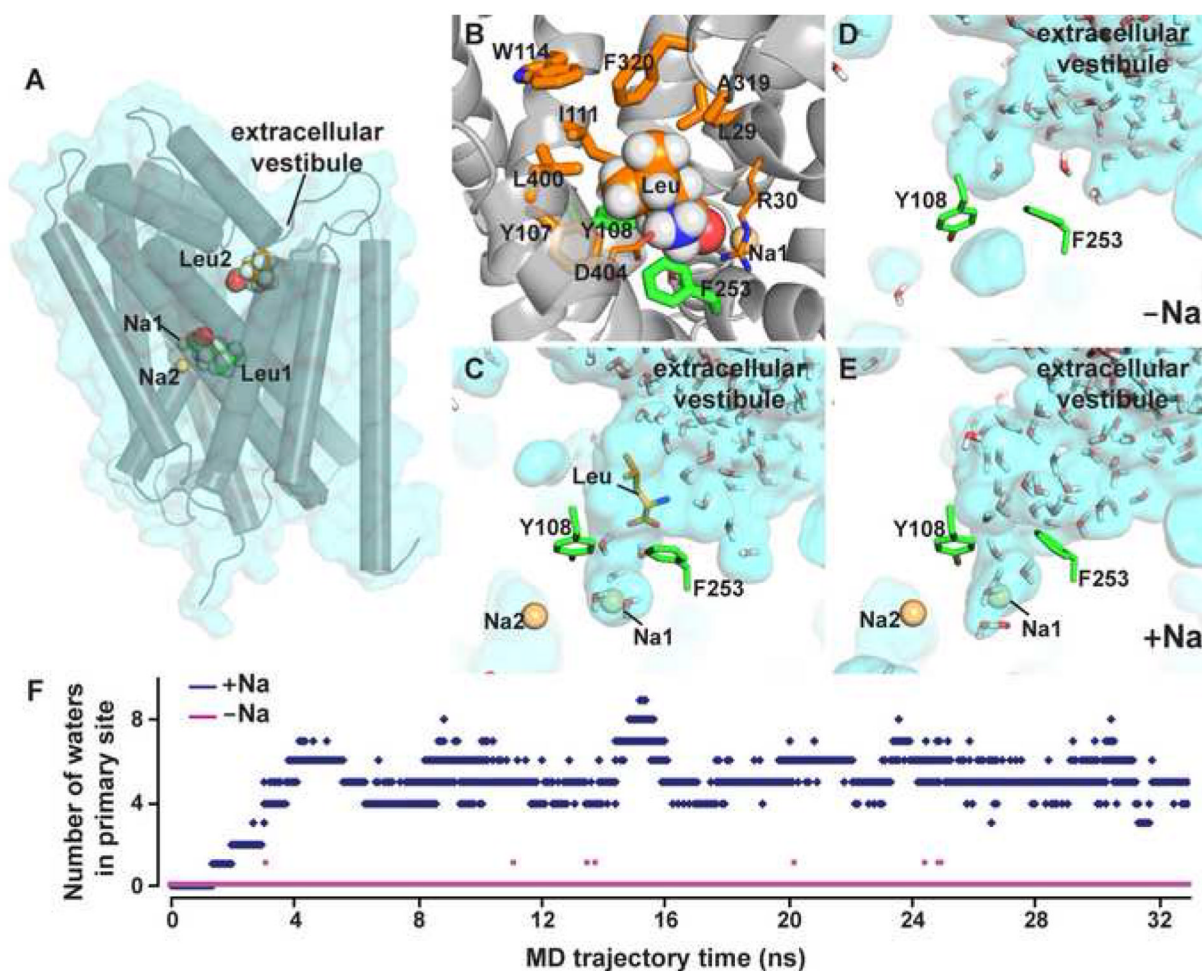


Figure 1.

The secondary substrate binding site in LeuT identified from SMD simulations and the role of Na^+ in the accessibility of the primary site. **A)** Side view (perpendicular to the membrane) of a LeuT model (TM helices are shown in cylinder representations) indicating the relative positions of the two binding sites. The secondary binding site is located at the bottom of the extracellular vestibule. **B)** Zoomed-in view of the residues forming the secondary site (in orange); Tyr108^{3,50} and Phe253^{6,53} (in green) line the route connecting the primary site to the secondary site in the SMD simulation (TM11 is omitted to reveal the internal perspective). The charged pair Arg30-Asp404 is shown in thinner stick rendering. **C-E)** Views of transparent molecular surfaces from the same perspective for various SMD simulation endpoints. Panel **C** shows a representative result from MD equilibration of a final conformation from SMD. Panels **D** and **E** represent the average structures of the “-Na/-Leu” and “+Na/-Leu” configurations, respectively. **F)** Time-dependent change in the number of water molecules in the primary binding site calculated from the trajectories of “-Na/-Leu” and “+Na/-Leu”, respectively. Note that water fills the primary site in the presence of Na^+ , but not in the absence of Na^+ . The water entry route in **E** is consistent with the substrate exit route in **C**.

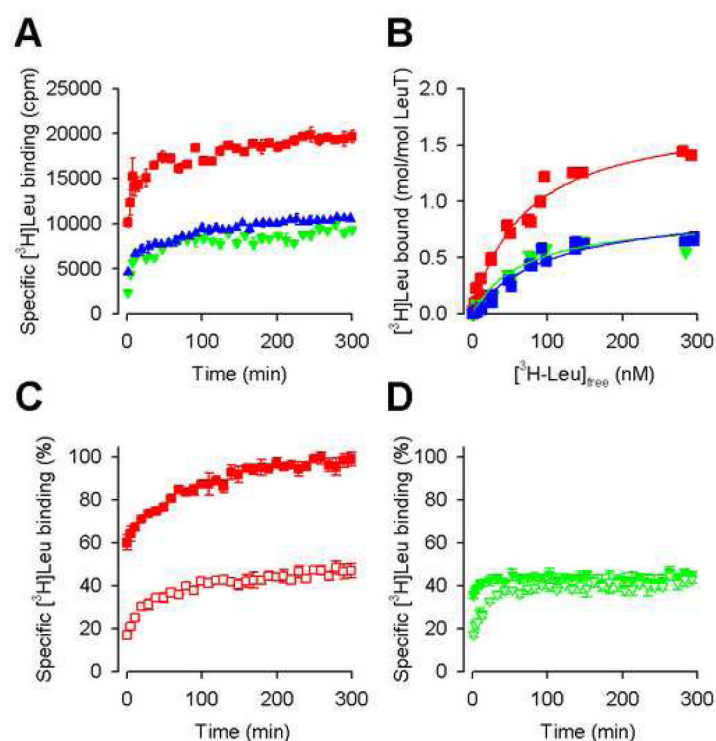


Figure 2.

Measurement of two Leu binding sites in LeuT. **A)** Time course of 100 nM 3 H-Leu binding by WT (■), I111C (▲), and L400C (▼). The half time for binding to equilibrium was 3.7 ± 1 min ($n=5$) for WT, and 5.3 ± 2.2 min ($n=5$) and 9.6 ± 7.5 min ($n=2$) for L400C and I111C, respectively. **B)** Stoichiometry of Leu binding. 3 H-Leu binding by WT, I111C, and L400C was assayed with 25 ng protein. Three independent experiments were subjected to global fitting in Prism and results of the fits are also shown in Results. **C, D)** Effect of CMI on Leu association. The time course of 100 nM 3 H-Leu binding by WT (**C**, □, ■) and L400C (**D**, ▼, ▽) was measured in the absence (■, ▼) and presence (□, ▽) of 1 mM CMI. Panels **A**, **C**, and **D** show representative experiments that were repeated at least three times and error bars indicate the mean \pm S.D. of triplicates.

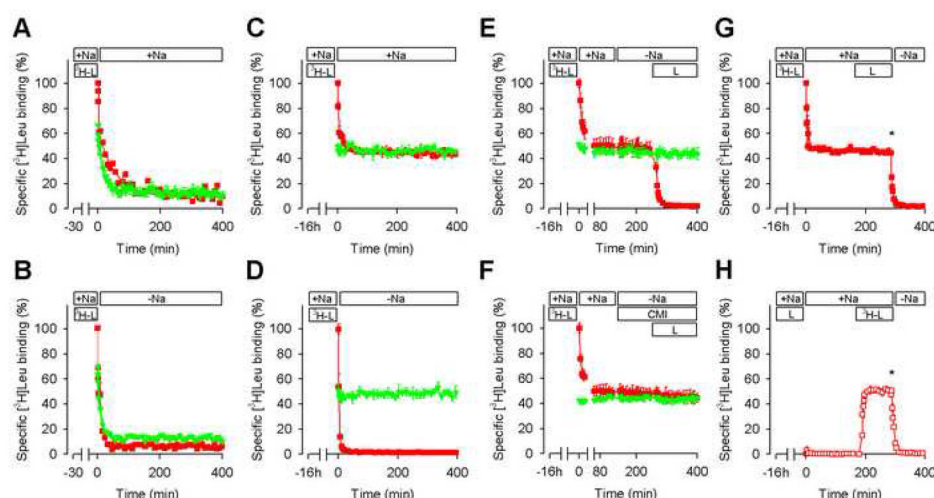


Figure 3.

Trapping of Leu in the primary binding site. **A, B**) Dissociation of 100 nM ^3H -Leu (^3H -L) from WT (■) and L400C (▼) after a 30-min incubation in the presence of 50 mM NaCl (+Na) by dilution in 50 mM NaCl (+Na; **A**) or NaCl-free media (-Na; **B**). Data points were normalized to the specific binding of WT after a 30-min incubation period. **C, D**) Dissociation of 100 nM ^3H -Leu after a 16-h incubation. The same experimental conditions as in **A** and **B** were applied and data points were normalized to WT specific binding after 16 h. **E**) Release of trapped ^3H -Leu is triggered by the addition of Leu in the absence of NaCl. After an 16-h incubation of WT or L400C in the presence of 100 nM ^3H -Leu and 50 mM NaCl, the samples were diluted in 50 mM NaCl-medium (+Na), followed by dilution in NaCl-free medium (-Na) and the addition of 250 nM Leu (L). **F**) Effect of CMI on trapped ^3H -Leu release. The same experiment as in **E** was performed except that the second dilution was in NaCl-free buffer containing 1 mM CMI. Symbol usage is consistent in **A–F**. **G, H**) Release of ^3H -Leu from the S1 and S2 sites (see text for details) exhibits different dissociation kinetics. After a 16-h incubation of LeuT-WT with 100 nM ^3H -Leu (**G**) or 500 nM Leu (**H**) in the presence of 50 mM NaCl, the samples were diluted in 50 mM NaCl medium (+Na) to release bound S2. After reaching steady-state binding levels, the empty S2 site was refilled with 100 nM Leu (**G**) or 100 nM ^3H -Leu (**H**). Dilution of the equilibrated samples in NaCl-free medium (-Na) caused release of S1 and S2. Thus, the dissociation of S1 is monitored in panel **G**, whereas the dissociation of S2 is monitored in panel **H**. The star in panel **G** and **H** indicates the 0 min point of the time-normalized data in Fig. S7. Panels **A–H** show representative experiments that were repeated at least three times and error bars indicate the mean \pm S.D. of triplicates.

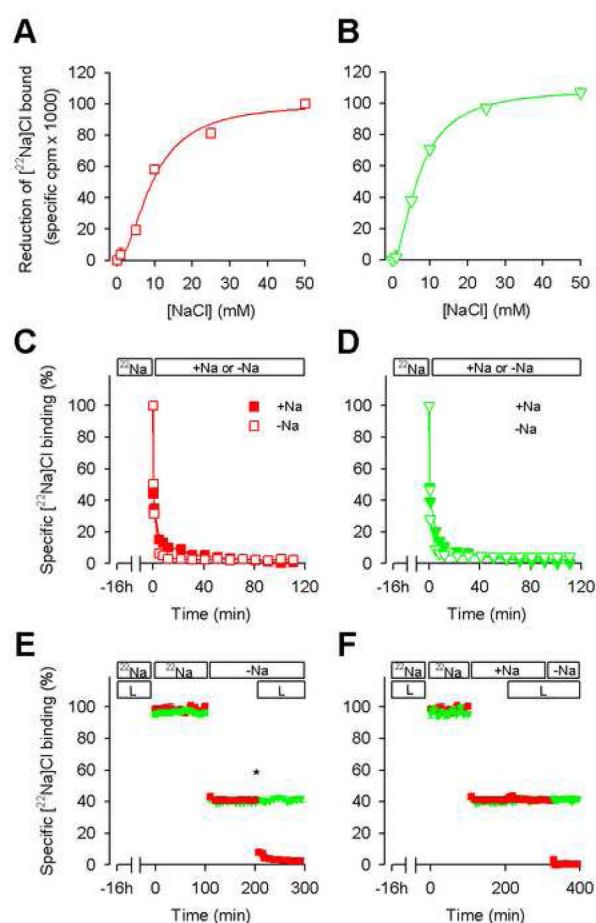
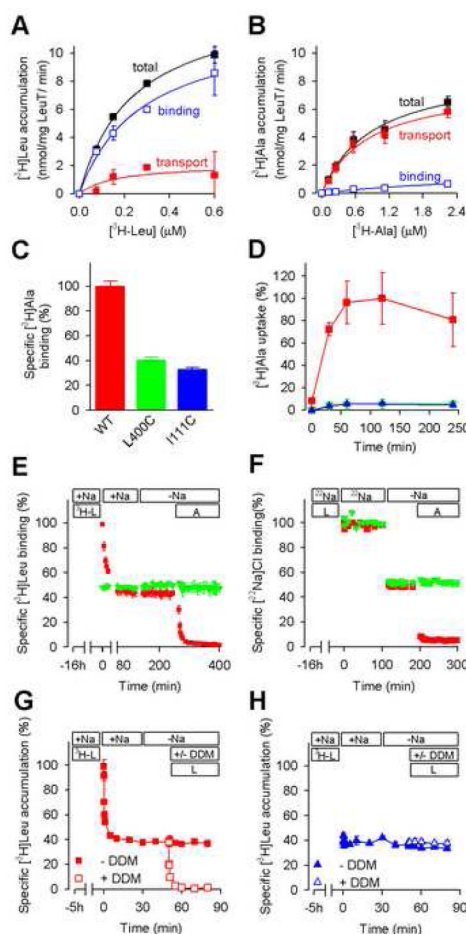


Figure 4.

Na⁺ binding kinetics. **A, B** 2 μM ²²NaCl binding by LeuT-WT (**A**) and L400C (**B**) was measured with 0-50 mM unlabelled NaCl. Data of two independent experiments were fitted to the Hill equation and the $IC_{50}^{Na^+}$ and Hill coefficients were shown as mean ± SEM in the Results. Panels **C-F** depict representative experiments. **C, D** Dissociation kinetics of LeuT-WT (**C**, ■, □) and L400C (**D**, ▼, ▽) after a 16-h incubation in the presence of 2 μM ²²NaCl by dilution in 50 mM unlabeled NaCl medium (■, ▼, +Na) or in NaCl-free medium (□, ▽, -Na). **E, F**. After a 16-h incubation in the presence of 2 μM ²²NaCl and 250 nM Leu, LeuT-WT (■) and L400C (▼) were diluted into 2 μM ²²NaCl-containing medium followed by dilution into NaCl-free medium (-Na, **E**) or 50 mM NaCl-containing buffer (+Na, **F**) and the addition of 250 nM Leu (in panel **F** another dilution was done into NaCl-free buffer in the presence of 250 nM L-Leu). The star in panel **E** indicates the 0 min point of the time normalized data in Fig. S7. Panels **A-F** show representative experiments that were repeated at least two times and error bars indicate the mean ± S.D. of triplicates.

**Figure 5.**

The secondary site is essential for transport. **A, B**) The activity of LeuT-WT reconstituted into PLs was determined by ^3H -Leu (**A**) and ^3H -Ala (**B**) accumulation with increasing concentrations of either substrate. Measurements were performed in the presence of an inwardly directed Na^+ electrochemical gradient (50 mM external NaCl; \blacksquare , total accumulation) or by dissipation of the gradient with 25 μg gramicidin/mL (\square , specific binding) added 5 min prior to the start of the reaction. Specific substrate transport (\blacksquare) was determined by the difference of total accumulation and specific binding to exhibit a K_m^{Leu} of 0.16 ± 0.21 μM and $V_{\text{max}}^{\text{Leu}}$ of 2.1 ± 1 nmol Leu/mg LeuT/min and a K_m^{Ala} of 0.82 ± 0.16 μM and a $V_{\text{max}}^{\text{Ala}}$ of 8.8 ± 0.7 nmol Ala/mg LeuT/min. **C**) Functional reconstitution of WT (red), L400C (green), and I111C (blue) into proteoliposomes was confirmed by binding of 2 μM ^3H -Ala in the presence 50 mM NaCl and gramicidin for 30 min. **D**) Impaired transport by secondary site mutants. Time course of specific ^3H -Ala (2 μM final concentration) transport by WT (\blacksquare), L400C (\blacktriangledown), and I111C (\blacktriangle) in PLs in the presence of external 50 mM NaCl. **E, F**) Release of trapped ^3H -Leu (**E**) or $^{22}\text{NaCl}$ (**F**) from WT was triggered by 5 μM Ala. Experimental conditions were identical to those shown in Fig. 3E and Fig. 4E, respectively, with the exception that Ala was used instead of Leu. **G, H**) Trapped ^3H -Leu was released into the lumen of LeuT-WT PLs (**G**) by the addition of external 250 nM Leu (L) as determined by the loss of radiotracer upon permeabilization of the PLs with 0.05 % (w/v) n-dodecyl- β -D-maltopyranoside (DDM). Externally added Leu failed to trigger release of trapped ^3H -Leu in PLs with the secondary site mutant L400C (**H**). Total ^3H -Leu accumulation was corrected for nonspecific accumulation

in control liposomes. All panels show representative experiments that were repeated two to four times and errors indicate the mean \pm SD of triplicates.

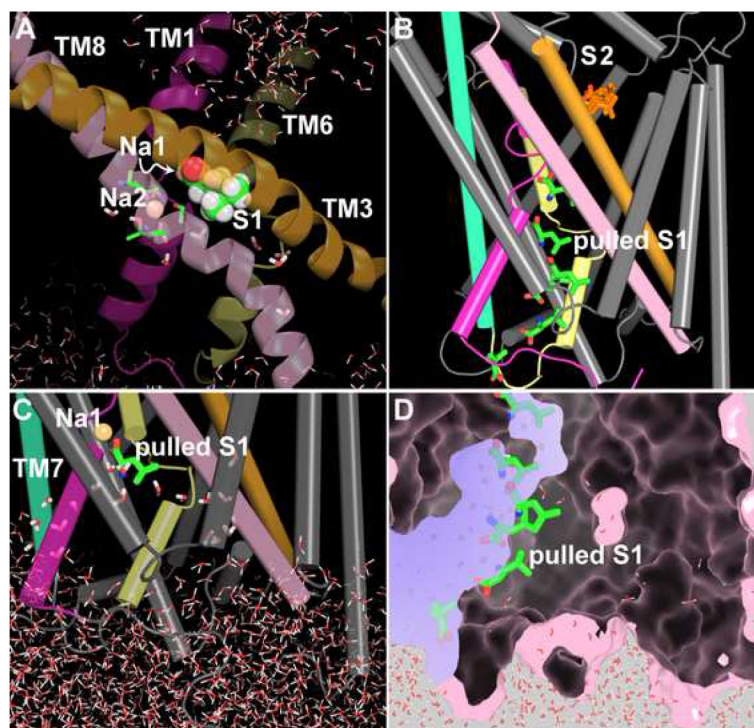


Figure 6.

Na2 and the intracellular transport pathway. **A)** Positioned at the intersection of the transmembrane segments forming the primary substrate binding site (S1 shown in CPK representation), Na2 has a key role in organizing this region of the transporter. The S1 binding segments TM1, 3, 6, and 8 are shown as ribbons, with Na2 binding residues shown in stick rendering. **B)** The representative poses of S1 (shown in green stick rendering) at different equilibration points from two parallel runs of SMD pulling in the inward (intracellular) direction. These positions are distributed along the SMD pathway, which represents the presumed intracellular substrate translocation pathway (see Supplemental Table 1 for the residues swept in the pathway). The transmembrane segments are shown as cylinders and TMs 1,3,6, and 8 are colored as in **A**. **C)** Viewed from the same angle as in **B**, significant water penetration from the intracellular milieu observed in the pathway at the end of the first stage SMD pulling of S1 (see Supplemental Experimental Procedures). Water molecules penetrate from several directions, including the region between intracellular segments of TMs 1 and 7. **D)** Shown from the same perspective as in **C**, the equilibrated structure of a second-stage SMD run is represented as surface rendering obtained as described for Fig. 7. An intracellular water tunnel is formed, which is highlighted in light blue, and the progression of the ligand is represented by its position at several points in the SMD trajectory.

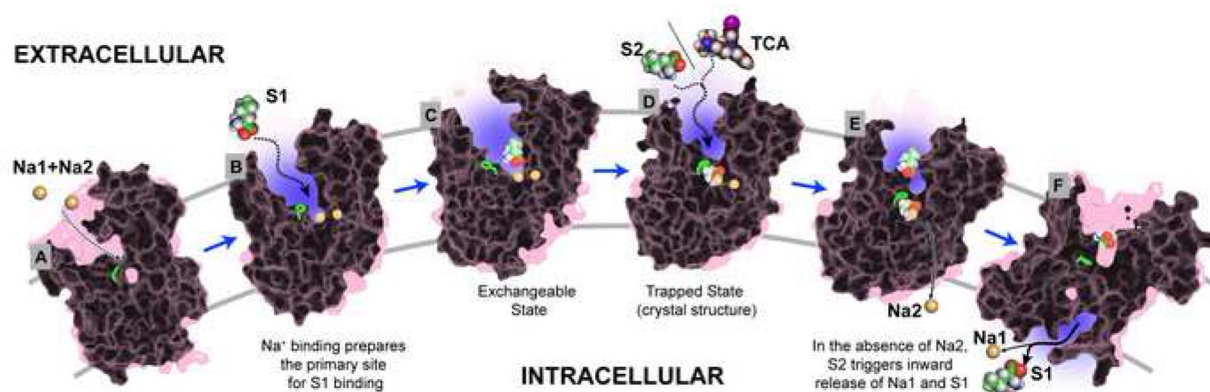


Figure 7.

Schematic model of the proposed Na⁺-coupled symport by LeuT. One of the key residues located between the primary and secondary sites, Phe253^{6,53}, is shown as a stick model in green because conformational changes in both its backbone and rotamer angles (χ^1 rotamer from *gauche* (C) to *trans* (D)) are involved in closing the primary site to the extracellular milieu. The transporter models are in molecular surface representations that are sliced open along the proposed transport pathway (shown in greater detail in Figs. 1 & 6). A binding/unbinding event that is poised to happen, or has occurred, is indicated by a dotted or a solid arrow, respectively. Water accessible regions are shown as blue areas.